THE ASTROPHYSICAL JOURNAL, 484:439–454, 1997 July 20

JOINT INSTABILITY OF LATITUDINAL DIFFERENTIAL ROTATION AND TOROIDAL MAGNETIC FIELDS BELOW THE SOLAR CONVECTION ZONE

PETER A. GILMAN AND PETER A. FOX
High Altitude Observatory, National Center for Atmospheric Research,[1] P.O. Box 3000, Boulder, CO 80307;
gilman@ucar.edu, pfox@ucar.edu
Received 1996 November 26; accepted 1997 February 7

ABSTRACT

Below the convection zone, where the stratification is radiatively controlled, large-scale motions should be mainly horizontal, i.e., in spherical shells due to the stabilizing effect of negative buoyancy on radial displacements. Watson showed that the observed surface solar differential rotation is at the threshold for instability to horizontal disturbances. Therefore, since helioseismology tells us the latitudinal differential rotation below the convection zone is less than the surface value, the profile should be stable too. We show that in the presence of a broad, nonuniform toroidal field the solar differential rotation is unstable. This is true for a wide range of kinetic and magnetic energies of the unperturbed state, from well below equipartition to well above it. We find instability for essentially all values of differential rotation and toroidal fields for which we are able to find converged solutions. The instability appears to occur only for longitudinal wave number 1. Disturbance symmetries about the equator and profiles in latitude depend on the amplitude of the toridal field. Peak *e*-folding times are a few months. The primary energy source for the instability is differential rotation for low field strengths and the toroidal field for high field strengths. The mechanism of energy release from the differential rotation is the poleward transport of angular momentum, by the Maxwell stress rather than the Reynolds stress. For the profiles studied, the Reynolds stress is almost always trying to rebuild differential rotation, the exact opposite of the nonmagnetic case. Second-order perturbation theory predicts that the unstable modes produce zonal jets and fine structure in the toroidal field, the latitude of which migrates toward the equator with increasing magnetic field strength. The instability we have found may play a role in the solar dynamo, although being two-dimensional, it cannot produce a dynamo by itself. Mixing of angular momentum caused by the instability could allow achievement of equilibrium of the solar tachocline hypothesized by Spiegel & Zahn.

Subject headings: hydrodynamics — instabilities — MHD — Sun: interior — Sun: magnetic fields — Sun: rotation

1. INTRODUCTION

Helioseismological measurements and inversions (Brown et al. 1989; Goode et al. 1991; Tomczyk, Schou, & Thompson 1995) indicate that there is a layer at or near the base of the convection zone where the latitudinal differential rotation of the photosphere and convection zone declines in amplitude to solid rotation at a value intermediate between that of the solar equator and pole at the surface. This layer therefore must contain a substantial radial gradient of angular velocity, of opposite signs in low and high latitudes.

It is widely suspected that the angular velocity gradients of this layer are a principal driver of the solar dynamo responsible for the solar magnetic cycle. Effective dynamo action from such gradients also requires a substantial residence time for the magnetic field. This means that the effects of magnetic buoyancy must be at least partially neutralized. The convection zone, itself buoyantly unstable by definition, provides no real mechanism; however, the layers immediately underneath, where the radial temperature gradient is less than adiabatic, can store the fields for extended periods. This is particularly true below the convection zone where the temperature gradient is determined by radiation balance, i.e., below the depth of overshooting of convective elements. It is this layer to which the theory that follows here is best applied.

The most recent estimates from helioseismology (Kosovichev 1996) place about $\frac{3}{4}$ of the shear layer in the radiative region below the solar convection zone. The total thickness of the shear layer is estimated as 0.09 ± 0.04 of the solar radius with midpoint at 0.692 ± 0.005 of the radius. These estimates are of course subject to revision based on more extensive helioseismological data that is now being produced by the Global Oscillations Network Group (GONG) program and the *Solar and Heliospheric Observatory* (*SOHO*) satellite, but it seems likely that a substantial fraction of the shear layer will still be found to reside below the convection zone.

In the presence of strong negative buoyancy, global fluid motions will be largely confined to spherical shells. Differential rotation itself is perhaps the simplest form of such a motion, but other more complex flows could also exist, particularly flows with longitudinal dependence. A possible origin of such flows is instability of the latitude gradient of rotation, which grows by taking momentum from latitudes where it is high to where it is low, thus extracting kinetic energy. For the sun this would mean transporting angular momentum from low latitudes to high.

The existence of a two-dimensional instability of differential rotation was first demonstrated in the context of the global circulation of the Earth's atmosphere (Kuo 1949). It required there be an extremum in the vorticity of the flow. Watson (1981) investigated this stability problem for solar-type differential rotation profiles and showed that, for differential rotation between equator and pole of about 29%

[1] The National Center for Atmospheric Research is sponsored by the National Science Foundation.

or more, the profile is indeed unstable, particularly to longitudinal wave number $m = 1$. Below that limit, the profile is stable to all wavenumbers. Watson concluded that this instability might cause the photospheric differential rotation of the Sun to be limited to about 30%.

Watson of course did not know about the shear layer at the base of the convection zone where the theory is more applicable because of the highly stable stratification there. But since the latitudinal differential rotation is significantly less than 30% at these depths, Watson's result would imply that the latitudinal gradient should be stable. Spiegel & Zahn (1992) developed a theory for the radial gradient of rotation beneath the convection zone (which they call the solar tachocline) that requires highly anisotropic mixing of angular momentum below the convection zone, with much stronger latitudinal than radial exchange. (With isotropic eddy mixing of momentum, the radial gradient would have diffused all the way to the core in a time short compared to the age of the Sun.) But such enhanced latitudinal mixing can really only come from an instability of the differential rotation profile, which, according to Watson, is stable. How is this paradox to be resolved?

Spiegel & Zahn did not consider the effect of magnetic fields. We show here that a toroidal magnetic field can render the differential rotation unstable. This is true for a very wide range of field strengths and for differential rotations that are much less than the photospheric value. The instability provides angular momentum mixing in latitude, but through the Maxwell stress rather than the Reynolds stress.

Coexisting shear flow and parallel magnetic fields in Cartesian geometry, each separately stable, have previously been found to be unstable by Stern (1962) and Kent (1968). The instability we have discussed here should be related to that discussed by Balbus & Hawley (1994), except that our analysis is global while theirs is local, and some of the physics is different; no detailed comparison has been made yet. We do note that while the Balbus & Hawley instability draws energy only from differential rotation, we will demonstrate that ours takes it from both differential rotation and the toroidal field.

We present in this paper the basic formulation of the stability problem, as a hydromagnetic extension of the analysis of Watson (1981), and demonstrate the existence of the instability with solutions for simple toroidal field profiles. Later papers in the series will give results for more complex profiles, as well as for inclusion of additional physics.

2. PHYSICAL ASSUMPTIONS AND GOVERNING EQUATIONS

In this initial study of the instability, we simplify the physics as much as possible. We treat the problem as an "ideal MHD" generalization of the analysis carried out by Watson (1981) for the nonmagnetic case. Nevertheless, we believe the physics retained still defines a fairly realistic problem for the shear layer at the base of the convection zone of the sun.

Following Watson, we treat the problem as strictly two-dimensional, with reference state and perturbations lying in a spherical shell, with no radial variations. Viscous and ohmic diffusion are ignored. This also should be a good approximation for disturbances with substantial growth rates. Compressibility is also ignored since the two-dimensional assumption precludes radial displacements and the relevant timescales for extraction of energy from the differential rotation and/or toroidal field are very long compared to any relevant sound travel time.

We use longitude (λ) and latitude (ϕ) coordinates, define velocity $= u\hat{\boldsymbol{\lambda}} + v\hat{\boldsymbol{\phi}}$ and magnetic field $= a\hat{\boldsymbol{\lambda}} + b\hat{\boldsymbol{\phi}}$. It is convenient to use a modified pressure variable $\pi = p/\rho$, in which p and ρ are the ordinary pressure and density, respectively. Then, we can write the nonlinear governing equations that have the density, shell radius, and factors of 4π in the $\boldsymbol{j} \times \boldsymbol{B}$ force scaled out, as continuity equations for velocity and magnetic field, two equations of motion, and two induction equations:

$$\frac{\partial u}{\partial \lambda} + \frac{\partial}{\partial \phi}(v \cos \phi) = 0 , \tag{1}$$

$$\frac{\partial a}{\partial \lambda} + \frac{\partial}{\partial \phi}(b \cos \phi) = 0 , \tag{2}$$

$$\frac{\partial u}{\partial t} + \frac{1}{\cos \phi}\frac{\partial}{\partial \lambda}\left(\frac{u^2 + v^2}{2}\right) - \frac{v}{\cos \phi}\left[\frac{\partial}{\partial \lambda} v - \frac{\partial}{\partial \phi}(u \cos \phi)\right] = -\frac{1}{\cos \phi}\frac{\partial \pi}{\partial \lambda} - \frac{b}{\cos \phi}\left[\frac{\partial b}{\partial \lambda} - \frac{\partial}{\partial \phi}(a \cos \phi)\right], \tag{3}$$

$$\frac{\partial v}{\partial t} + \frac{\partial}{\partial \phi}\left(\frac{u^2 + v^2}{2}\right) + \frac{u}{\cos \phi}\left[\frac{\partial}{\partial \lambda} v - \frac{\partial}{\partial \phi}(u \cos \phi)\right] = -\frac{\partial \pi}{\partial \phi} + \frac{a}{\cos \phi}\left[\frac{\partial}{\partial \lambda} b - \frac{\partial}{\partial \phi}(a \cos \phi)\right], \tag{4}$$

$$\frac{\partial a}{\partial t} - \frac{\partial}{\partial \phi}(ub - va) = 0 , \tag{5}$$

$$\frac{\partial b}{\partial t} + \frac{1}{\cos \phi}\frac{\partial}{\partial \lambda}(ub - va) = 0 . \tag{6}$$

Equation (2) can be derived from equations (5) and (6), so there are actually only five independent equations for the five unknowns.

3. EXPANSION INTO REFERENCE STATE AND PERTURBATION EQUATIONS

We separate the dependent variables into a reference state, which is independent of longitude (denoted by an overbar) and perturbations (denoted by primes). Thus,

$$\pi = \bar{\pi} + \pi', \quad u = \bar{u} + u', \quad v = v', \quad a = \bar{a} + a', \quad b = b' . \tag{7}$$

From equations (1) and (2) $\bar{v}$ and $\bar{b}$ vanish because of the assumptions of two-dimensionality. Then we expand the governing equations into zeroth-, first-, and second-order components. Zeroth order simply relates the reference state "pressure" $\bar{\pi}$ to a specified $\bar{a}$ and $\bar{u}$ according to

$$\frac{\partial}{\partial \phi}\left(\bar{\pi} + \frac{\bar{a}^2}{2}\right) = (\bar{a}^2 - \bar{u}^2) \tan \phi , \tag{8}$$

from equation (4).

The first-order system gives the perturbation equations:

$$\frac{\partial u'}{\partial \lambda} + \frac{\partial}{\partial \phi}(v' \cos \phi) = 0 , \tag{9}$$

$$\frac{\partial a'}{\partial \lambda} + \frac{\partial}{\partial \phi}(b' \cos \phi) = 0 , \tag{10}$$

$$\frac{\partial u'}{\partial t} + \frac{1}{\cos\phi}\frac{\partial}{\partial\lambda}(\bar{u}u') + \frac{v'}{\cos\phi}\frac{\partial}{\partial\phi}(\bar{u}\cos\phi) = -\frac{1}{\cos\phi}\frac{\partial\pi'}{\partial\lambda} + \frac{b'}{\cos\phi}\frac{\partial}{\partial\phi}(\bar{a}\cos\phi), \quad (11)$$

$$\frac{\partial v'}{\partial t} + \frac{\partial}{\partial\phi}(\bar{u}u') + \frac{\bar{u}}{\cos\phi}\frac{\partial v'}{\partial\lambda} - \frac{\bar{u}}{\cos\phi}\frac{\partial}{\partial\phi}(u'\cos\phi) - \frac{u'}{\cos\phi}\frac{\partial}{\partial\phi}(\bar{u}\cos\phi) = -\frac{\partial\pi'}{\partial\phi} + \frac{\bar{a}}{\cos\phi}\frac{\partial b'}{\partial\lambda} - \frac{\bar{a}}{\cos\phi}\frac{\partial}{\partial\phi}(a'\cos\phi) - \frac{a'}{\cos\phi}\frac{\partial}{\partial\phi}(\bar{a}\cos\phi), \quad (12)$$

$$\frac{\partial a'}{\partial t} = \frac{\partial}{\partial\phi}(\bar{u}b' - \bar{a}v'), \quad (13)$$

$$\frac{\partial b'}{\partial t} = -\frac{1}{\cos\phi}\frac{\partial}{\partial\lambda}(\bar{u}b' - \bar{a}v'). \quad (14)$$

Subtracting the first-order perturbation equations (11) and (13) from the full equations (3) and (5) in expanded form and then averaging over λ allow us to compute initial tendencies for the change in the reference states $\bar{a}$ and $\bar{u}$, as second-order quantities, resulting from the "stresses" or correlations among perturbation variables.

$$\frac{\partial\bar{u}}{\partial t} = \frac{1}{\cos^2\phi}\frac{\partial}{\partial\phi}[\cos^2\phi(\overline{a'b'} - \overline{u'v'})], \quad (15)$$

$$\frac{\partial\bar{a}}{\partial t} = \frac{\partial}{\partial\phi}(\overline{u'b'} - \overline{v'a'}). \quad (16)$$

The balance equation (8) for the reference state pressure $\bar{\pi}$ also changes to second order, but we omit the details since we have no need to refer to it in this paper.

The correlation $\overline{u'v'}$ is the Reynolds stress, responsible for extracting energy from the differential rotation in Watson (1981) stability analysis; the correlation $\overline{a'b'}$ is the Maxwell stress, which is obviously capable of doing the same thing. A key point, though, is that $\overline{u'v'}$ and $\overline{a'b'}$ appear with opposite signs, so the same functional shape of velocity and magnetic disturbances will transport momentum in opposite directions. We will see this compensating tendency at work in our solutions. We will call the correlation $\overline{u'b'} - \overline{v'a'}$ the "mixed" stress, which from equation (16) provides the only mechanism in the two-dimensional ideal MHD case for extracting energy from the reference state toroidal field.

4. REDUCTION OF PERTURBATION EQUATIONS TO A SOLVABLE SYSTEM

Since the perturbations are two-dimensional, we can satisfy the continuity equations (9) and (10) identically by representing u', v', and a', b' by "stream functions" ψ and χ, respectively:

$$u' = -\frac{\partial\psi}{\partial\phi}, \quad v' = \frac{1}{\cos\phi}\frac{\partial\psi}{\partial\lambda},$$

$$a' = -\frac{\partial\chi}{\partial\phi}, \quad b' = \frac{1}{\cos\phi}\frac{\partial\chi}{\partial\lambda}.$$

In addition, it is convenient to rewrite $\bar{u}$ and $\bar{a}$ in the form,

$$\bar{u} = \omega_0\cos\phi, \quad \bar{a} = \alpha_0\cos\phi,$$

so that ω_0 is the total angular frequency and α_0 is a magnetic analog. Then, assuming perturbation variables ψ and χ are proportional to $e^{im(\lambda - ct)}$, m an integer, and substituting $\mu = \sin\phi$, the perturbation equations (9)–(14) can be reduced to a pair of ordinary differential equations

$$(\omega_0 - c)L\psi - \psi\frac{d^2}{d\mu^2}[\omega_0(1-\mu^2] - \alpha_0 L\chi + \chi\frac{d^2}{d\mu^2}[\alpha_0(1-\mu^2)] = 0, \quad (17)$$

$$(\omega_0 - c)\chi = \alpha_0\psi. \quad (18)$$

In equation (17)

$$L(\ ) = \frac{d}{d\mu}\left[(1-\mu^2)\frac{d}{d\mu}(\ )\right] - \frac{m^2}{1-\mu^2}(\ )$$

is the "Legendre operator" as defined by Watson.

As in Watson (1981), we assume $\psi = 0$ at the poles, and therefore from equation (18) $\chi = 0$ there also. These conditions are necessary to avoid nonphysical singularities there. Flow and field are still allowed across the poles, when $m = 1$.

Watson solved equation (17) with $\alpha_0 = 0$ by expanding in associated Legendre polynomials. We generalize this approach to the hydromagnetic system (17)–(18).

5. INTEGRAL THEOREMS

Without solving equations (17) and (18) in detail, there are certain statements that can be made about unstable solutions from integrals of these equations. Watson (1981) derived several of these for the nonmagnetic case, based on an earlier extensive review by Drazin & Howard (1966). In the MHD case, some of the integral constraints for unstable modes contain many terms and are not particularly enlightening. We briefly select results that will be of use in interpreting our solutions. In particular, if we introduce the transformation $\psi = (\omega_0 - c)H$, multiply equation (17) by H^*, substitute for χ from equation (18), integrate from pole to pole, and integrate by parts, applying the pole condition $\psi = 0$, we obtain

$$\int_{-1}^{1}[(\omega_0 - c)^2 - \alpha_0^2]\left[(1-\mu^2)\left|\frac{dH}{d\mu}\right|^2 + \frac{m^2}{1-\mu^2}|H|^2\right]d\mu = \int_{-1}^{1}\left\{2(\omega_0 - c)c + \frac{1}{\mu}\frac{d}{d\mu}\mu^2[(\omega_0 - c)^2 - \alpha_0^2]\right\}|H|^2\,d\mu. \quad (19)$$

Separating out the imaginary part gives

$$c_i\left\{\int_{-1}^{1}(\omega_0 - c_r)\left[(1-\mu^2)\left|\frac{dH}{d\mu}\right|^2 + \frac{m^2}{1-\mu^2}|H|^2\right]d\mu - \int_{-1}^{1}\frac{d}{d\mu}(\mu\omega_0)|H|^2\,d\mu\right\} = 0. \quad (20)$$

So for unstable modes to exist, the sum of integrals inside the braces in equation (20) must vanish. This places bounds on the phase velocity of unstable disturbances that are independent of the magnitude and profile of the toroidal field; so the bounds are the same as stated by Watson (1981). We

can solve equation (20) for c_r, in the form

$$c_r = \langle \omega_0 \rangle - \int_{-1}^{1} \frac{d}{d\mu}(\mu\omega_0)|H|^2 \, d\mu \Big/ \int_{-1}^{1} \left[(1-\mu^2)\left|\frac{dH}{d\mu}\right|^2 + \frac{m^2}{1-\mu^2}|H|^2 \right] d\mu \,, \quad (21)$$

in which $\langle \omega_0 \rangle$ is a weighted average of the differential rotation at all latitudes, given by

$$\langle \omega_0 \rangle = \int_{-1}^{1} \omega_0 \left[(1-\mu^2)\left|\frac{dH}{d\mu}\right|^2 + \frac{m^2}{1-\mu^2}|H|^2 \right] d\mu \Big/ \int_{-1}^{1} \left[(1-\mu^2)\left|\frac{dH}{d\mu}\right|^2 + \frac{m^2}{1-\mu^2}|H|^2 \right] d\mu \,. \quad (22)$$

Clearly $\langle \omega_0 \rangle$ falls between the maximum and minimum rotation of the shell. Furthermore, with $\omega_0 = r - s\mu^2$, which is what Watson chose and we will choose for our model of the solar differential rotation, $d/d\mu\ (\mu\omega_0) = r - 3s\mu^3$, so unless $s > r/3$ ($r = 1$, $s \leqq 0.29$ for the Sun), the ratio of integrals must always reduce the phase velocity further. Thus, for solar conditions the phase velocity of an unstable disturbance cannot exceed the maximum rotation rate of the system, regardless of the strength and profile of the magnetic field. Therefore, the Alfvén speed does not predominate in determining the phase velocity of unstable modes. Under certain conditions, from equation (21) the phase velocity would be slightly lower than the minimum rotation, but again by an amount that does not depend explicitly on the magnetic field parameter α_0. There are, of course, many neutral, oscillating modes that are solutions of equations (17) and (18). The Alfvén speed does enter into these modes, but we do not consider them further here.

Multiplication of equation (17) by ψ^*, integration over the shell and by parts also yields a necessary condition for instability. In the nonmagnetic case discussed in Watson (1981) this yields the classical Rayleigh (1880) and Fjørtoft (1950) conditions for instability. Rayleigh's condition requires that for instability, $(d^2/d\mu^2)[\omega_0(1-\mu^2)]$ must change sign at some latitude. This condition is a consequence of total vorticity being conserved in the system and says that the latitude gradient of the reference-state vorticity must change sign in the shell. In the MHD case, the necessary condition contains several more terms, each integrand of which is proportional to α_0^2 or product of derivatives of α_0 (the detailed formula is given in the Appendix). It is clear that with these extra terms (several of which have the factor $(\omega_0 - c_r)$, which from the discussion above certainly changes sign in the shell), Rayleigh's condition is relaxed, meaning that instability can occur even if there is no sign change in the vorticity gradient. And indeed, we do find instability of the differential rotation under these conditions. The reason this can occur is that the toroidal magnetic field breaks the constraint of conservation of vorticity.

However, the magnetic field is not always destabilizing because it is also possible to show from the necessary condition that as $m \to \infty$, the growth rates must approach zero. This is the stabilizing effect of the $\boldsymbol{j} \times \boldsymbol{B}$ force, which increases like m^2 as m increases.

Other integral theorems can be derived that place bounds on growth rates of unstable disturbances as generalizations of those found in Watson (1981), but these bounds are quite loose, i.e., much larger than the actual growth rates found here, so we do not reproduce these bounds here.

6. SOLUTION BY LEGENDRE POLYNOMIAL SERIES

The separation of longitude from latitude dependence in the equations means that solutions can be represented by separate series of associated Legendre polynomials for each longitudinal wave number m so ψ and χ can be written as

$$\psi = \sum_{n=m}^{\infty} \Psi_n^m P_n^m(\mu) \,, \quad \chi = \sum_{n=m}^{\infty} X_n^m P_n^m(\mu) \,.$$

Then, if we recognize that from the associated Legendre equation $LP_n^m = -n(n+1)P_n^m$, equations (17) and (18) become

$$-(\omega_0 - c) \sum_{n=m}^{\infty} n(n+1)\Psi_n^m P_n^m - \frac{d^2}{d\mu^2}[\omega_0(1-\mu^2)] \sum_{n=m}^{\infty} \Psi_n^m P_n^m + \alpha_0 \sum_{n=m}^{\infty} n(n+1) X_n^m P_n^m + \frac{d^2}{d\mu^2}[\alpha_0(1-\mu^2)] \sum_{n=m}^{\infty} X_n^m P_n^m = 0 \,, \quad (23)$$

$$(\omega_0 - c) \sum_{n=m}^{\infty} X_n^m P_n^m = \alpha_0 \sum_{n=m}^{\infty} \Psi_n^m P_n^m \,. \quad (24)$$

So the differential equation (17) becomes the algebraic equation (23).

In order to carry the problem further, we must assume specific profiles for ω_0 and α_0. Watson (1981) took $\omega_0 = r - s\mu^2$, which is a good representation of the solar differential rotation; so we shall also. We choose $\alpha_0 = a\mu + b\mu^3$, which is the simplest profile that is antisymmetric about the equator, the dominant symmetry on the sun, and which allows both signs of toroidal field in each hemisphere.

Provided we avoid singularities, the eigensystems (23) and (24) can be solved by matrix inversion methods. This should be possible for unstable modes, for which c is complex. Because of symmetry properties, there are actually two matrix equations: one for ψ symmetric, χ antisymmetric about the equator ($\mu = 0$), and the other for ψ antisymmetric, χ symmetric. We will generally refer to the first pair as the symmetric case, and the second as the antisymmetric case, according to the symmetry of ψ. Thus, the symmetric perturbations have the same symmetries about the equator as the reference state, and the same as the dominant symmetries of the observed solar differential rotation, and toroidal field as inferred from sunspot magnetic polarities. Symmetric ψ and χ have $n = m$ as the first term in their series, while antisymmetric ψ and χ have $n = m + 1$ as the first term. Subsequent terms in each series are spaced by 2 in n.

By collecting coefficients of like Legendre polynomials, again following Watson, equations (23) and (24) each yield seven term recursion relations defined in the Appendix. These act as generators of series of diagonals in the matrix equation for each symmetry, the eigenvalue of which is c, and whose eigenvector is the sequence of coefficients Ψ_n^m, X_n^m, for all n values included in the particular truncation level chosen. In the solutions that follow, we have taken between 80 and 200 terms in the series. All calculations were performed on a SUN SPARCStation 5.

In this first study, we find solutions for the case with $\alpha_0 = a\mu (b = 0)$. We have studied solutions with $r = 1$ and s

between 0.01 and 0.45 and a between 0 and 2.0, to show the full range of behavior. We have created a database of more than 3600 solutions which we sample for the results shown below. We focus on solutions with $s < 0.30$, for which no instability occurs in the nonmagnetic case.

Recall that $\alpha_0 = a\mu$ implies $\bar{a} = a\mu(1-\mu^2)^{1/2} = a \sin\phi \cos\phi$, probably the simplest possible toroidal field profile that is antisymmetric about the equator and 0 at the poles with the peak toroidal field at $\phi = 45°$. But even with this simple profile, we show that the s, a space contains a rich variety of unstable mode behavior. This is largely because in the MHD case there are two sources of energy for growing modes: kinetic energy of differential rotation and magnetic energy of the toroidal field. So far in this study, we have found that only $m = 1$ is unstable. All higher m's give only neutral oscillations, presumably because of the stabilizing influence of the $\boldsymbol{j} \times \boldsymbol{B}$ force for higher m.

7. ENERGETICS AS SOLUTION DIAGNOSTICS

To interpret solutions and to understand the physics of the system generally, it is useful to derive equations for the energetics of the system from the combination of first- and second-order equations. These equations are quite general: they apply even for finite amplitude perturbations, not necessarily represented by solutions proportional to $e^{im(\lambda - ct)}$, and for all ω_0 and α_0, not just the polynomial forms we have chosen. The equations describe the transfers of energy between various pairs of four energy reservoirs, two kinetic, two magnetic, two reference state, and two perturbation.

The reference state kinetic energy reservoir $\bar{K}$ and magnetic energy reservoir $\bar{M}$ are defined as

$$\bar{K} \equiv \int_{-1}^{1} \frac{(\omega_0 - \omega_r)^2}{2}(1-\mu^2)d\mu ,$$

$$\bar{M} \equiv \int_{-1}^{1} \frac{\alpha_0^2}{2}(1-\mu^2)d\mu ,$$

in which ω_r is the rotation rate of an appropriate reference frame. In numerical comparisions, we will use the solar rotation rate below the shear layer. The corresponding perturbation energy reservoirs are defined as

$$K' \equiv \int_{-1}^{1} \frac{\overline{u'^2} + \overline{v'^2}}{2} d\mu , \quad M' \equiv \int_{-1}^{1} \frac{\overline{a'^2} + \overline{b'^2}}{2} d\mu .$$

Then we can show, by forming energy equations from (11)–(16), integrating over μ, and integrating by parts, that the energetics of this system can be written in symbolic form as

$$\frac{\partial \bar{K}}{\partial t} = -(\bar{K}, K') - (\bar{K}, M') , \tag{25}$$

$$\frac{\partial \bar{M}}{\partial t} = -(\bar{M}, K') , \tag{26}$$

$$\frac{\partial K'}{\partial t} = +(\bar{K}, K') + (\bar{M}, K') - (K', M') , \tag{27}$$

$$\frac{\partial M'}{\partial t} = +(\bar{K}, M') + (K', M') . \tag{28}$$

In the above (E, F) denotes an integral measuring the rate of energy conversion from form E to form F. The specific integrals are defined as follows

$$(\bar{K}, K') = -\int_{-1}^{1} (1-\mu^2)\overline{u'v'} \frac{\partial \omega_0}{\partial \mu} d\mu ,$$

work done by the Reynolds stress ;

$$(\bar{K}, M') = \int_{-1}^{1} (1-\mu^2)\overline{a'b'} \frac{\partial \omega_0}{\partial \mu} d\mu ,$$

work done by the Maxwell stress ;

$$(\bar{M}, K') = \int_{-1}^{1} (\overline{u'b'} - \overline{v'a'}) \frac{\partial}{\partial \mu}(\alpha_0(1-\mu^2))d\mu ,$$

work done by the "mixed" stress ;

$$(K', M') = -\int_{-1}^{1} \alpha_0 \overline{v'j'} d\mu ,$$

work done against the perturbation latitudinal $\boldsymbol{j} \times \boldsymbol{B}$ force ,

in which

$$j' = \frac{\partial b'}{\partial \lambda} - (1-\mu^2)^{1/2} \frac{\partial}{\partial \mu}[a'(1-\mu^2)^{1/2}] .$$

Equations (25)–(28) can be visualized with a diagram, seen in Figure 1. The arrowhead direction denotes energy converted from the first form in the parentheses to the second. The integrals in (25)–(28) always appear twice, with opposite signs, in two equations, representing extraction from one reservoir that must be deposited into another. Thus, as we should expect to second-order, the total energy of the system, $\bar{K} + \bar{M} + K' + M'$, is conserved. Figure 1 illustrates clearly that not all energy reservoirs are linked directly. In particular, there is no direct link between $\bar{K}$ and $\bar{M}$, or between $\bar{M}$ and M'.

The missing link between $\bar{K}$ and $\bar{M}$ is a consequence of the differential rotation and toroidal field being parallel, so no energetic consequences are felt. If we included poloidal fields that are independent of longitude, there would be a link, which represents the stretching of poloidal into toroidal field by the differential rotation, commonly part of field reversing dynamos. Inclusion of such a poloidal field would prevent rigorous treatment of the stability problem in general, because the reference state would not be a steady

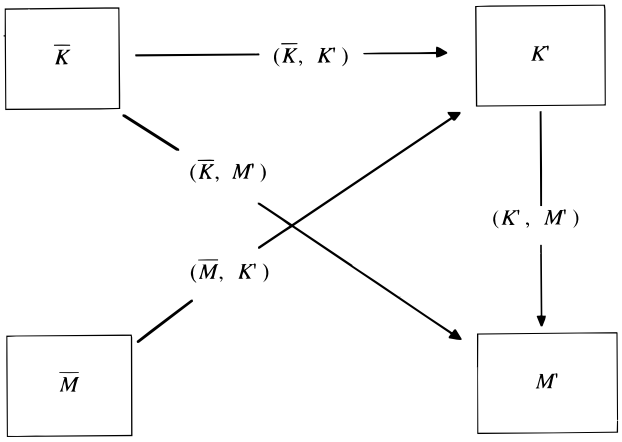

FIG. 1.—Schematic of possible conversions of energy among the four energy reservoirs in the system. Definitions given in § 7. Overbars denote reference state; primes denote perturbations.

solution of the governing equations, unless the poloidal field were everywhere parallel to isorotation surfaces. The missing link between $\bar{M}$ and M' is a consequence of the requirement that to extract energy from a magnetic reservoir requires a $\boldsymbol{j} \times \boldsymbol{B}$ force component to do work on the fluid, which in the first instance creates kinetic not magnetic energy. But then other components of the $\boldsymbol{j} \times \boldsymbol{B}$ force can be worked against by the fluid to create magnetic energy, which is what a positive value of (K', M') represents. It is of further interest to note from Figure 1 that while the Reynolds stress converts kinetic energy of differential rotation to perturbation *kinetic* energy, the Maxwell stress, which is always paired with the Reynolds stress (but of opposite sign) converts it to perturbation *magnetic* energy. So we should expect that the form of perturbation energy that is largest in growing disturbances is determined by which type of stress, Reynolds or Maxwell, is most effective at extracting energy from the differential rotation. We shall find that for $b = 0$ toroidal field profiles, the Maxwell stress nearly always wins, so the perturbation magnetic energy is always equal to or larger than the perturbation kinetic energy. The Reynolds stress in this case is always trying to rebuild the differential rotation, so the perturbation kinetic energy has to be built up from perturbation magnetic energy, through (K', M').

Some expectation for Maxwell stresses to predominate can be seen by examining the reference state kinetic energy equation, written in the form

$$\frac{\partial \bar{K}}{\partial t} = -2s \int_{-1}^{1} (1-\mu^2)(\overline{u'v'} - \overline{a'b'})\mu \, d\mu \, , \tag{29}$$

in which we have made use of $\omega_0 = r - s\mu^2$. From this expression, we see that net poleward transport of angular momentum by the Reynolds and/or Maxwell stresses, corresponding to $(\overline{u'v'} - \overline{a'b'}) > 0$, in the northern hemisphere, and < 0 in the southern, causes $\partial \bar{K}/\partial t < 0$, or extraction of energy from the differential rotation as we should expect. Now by substituting in the assumed form of the perturbations ψ and χ (§ 4) before the Legendre polynomial expansion, and using relation (18) to eliminate χ, we can show that

$$(\overline{u'v'} - \overline{a'b'}) = \left(1 - \frac{\alpha_0^2}{|\omega_0 - c|^2}\right)\overline{u'v'} + m \frac{\alpha_0^2 c_i |\psi|^2}{|\omega_0 - c|^4} s\mu \, , \tag{30}$$

in which the Maxwell stress is represented by the terms containing α_0^2. From the right-hand side of equation (30) we can see that for growing disturbances ($c_i > 0$) part of the Maxwell stress (second term on the right-hand side in (30) always transports momentum toward the poles at all latitudes. It is particularly large where the disturbance amplitude $|\psi|$ peaks, and where $|\omega_0 - c|^4$ is small. From the first term, we can also see that another part of the Maxwell stress always opposes the Reynolds stress and should dominate more and more as α_0 increases. This opposition comes from the tendency for perturbation velocities and magnetic fields to have similar structures with latitude since there is no diffusion present. The most likely scenario from (30) is that the Maxwell stress dominates, except perhaps when α_0 is small, and that it transports momentum towards the poles to extract energy from the differential rotation, while the Reynolds stress transports a smaller amount of momentum toward the equator. The detailed numerical solutions verify this inference.

A second statement can be made concerning instability from the reference magnetic energy equation (26). Using the same methods as just described above, plus additional integrations by parts, we find that

$$\frac{\partial \bar{M}}{\partial t} = \frac{mc_i}{2} \int_{-1}^{1} \frac{|\psi|^2}{|\omega_0 - c|^2} \left\{ \alpha_0 \frac{d^2}{d\mu^2} [(1-\mu^2)\alpha_0] \right\} d\mu \, . \tag{31}$$

From equation (31) we can immediately argue that for a growing perturbation ($c_i > 0$) to be deriving its energy from $\bar{M}$, so that $\partial \bar{M}/\partial t < 0$, it is necessary that $\alpha_0 \, d^2/d\mu^2[(1 - \mu^2)\alpha_0] < 0$ somewhere, and it is sufficient if this quantity is sufficiently negative. This criterion is of immediate interest for the case $\alpha_0 = a\mu$, i.e., $b = 0$, for then

$$\frac{\partial \bar{M}}{\partial t} = -\frac{3mc_i}{2} \int_{-1}^{1} \frac{|\psi|^2}{|\omega_0 - c|^2} a^2 \mu^2 \, d\mu \, . \tag{32}$$

Since the right-hand side of equation (32) is always negative for growing perturbations, such perturbations are getting at least some of their energy from the toroidal field. Of course, $\bar{M}$ need not be the primary energy source, and, indeed, we shall find that for the $\alpha_0 = a\mu$ profile, the toroidal field does not become the primary source until $a > 0.3$.

8. RESULTS

8.1. *Growth Rates of Unstable Disturbances*

Watson (1981) found that in the nonmagnetic case for $m = 1$, only the mode with ψ antisymmetric about the equator was unstable. By contrast, we find that in the presence of a toroidal field, both symmetries are excited: ψ symmetric and χ antisymmetric about the equator dominate when the toroidal field parameter a is small ($a \leq 0.3$), and ψ antisymmetric, χ symmetric prevail when the toroidal field is larger. Figures 2 and 3 show the growth rates for these cases for various values of s. The growth rates are given in dimensionless units, scaled by the equatorial rotation rate. A growth rate of 0.01 corresponds, in dimensional terms, to an e-folding growth time of about one year on the Sun. Therefore, it is clear from Figures 2 and 3 that disturbance growth times range between a few months and several years, depending on parameter values.

The uppermost curve in each figure is for $s = 0.3$ (approximately the photospheric differential rotation rate relative to the equatorial rotation rate). Each successive curve below that is decreased in s by 0.03, so the symmetric case goes down to $s = 0.15$ (50% of the photosphere), and the antisymmetric case goes down to $s = 0.09$ (30% of the photosphere). These lower limits do not represent stability boundaries but rather a more practical limit for this method of calculation, based on convergence and closeness to singularities in the complex plane. We cannot tell with this method precisely where in parameter space the stability boundary is because the smaller the growth rate, the more nearly singular the matrix becomes. It is possible that the instability disappears only in the limit of a going to zero. The fine structure in the growth rate curves in the symmetric case below $c_i = 0.005$ are caused by the near singular matrix being inverted and may not represent accurately the weak instability at these parameter values. The same is true for the fine structure for the antisymmetric case for $a \sim 0.3$.

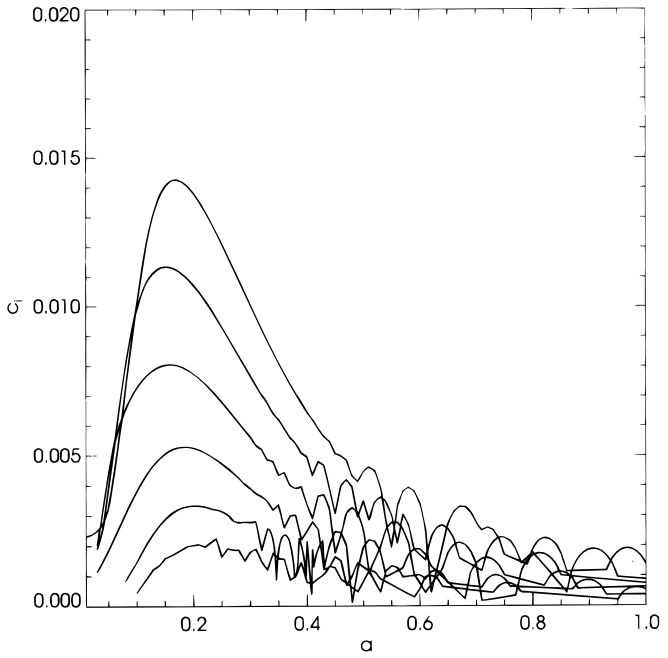

FIG. 2.—Growth rate c_i for symmetric modes (ψ symmetric, χ antisymmetric) as a function of toroidal field parameter a. Curves are for differential rotation parameter values $s = 0.30$–0.18 in decrements of 0.03, with $s = 0.30$ having the highest growth rate. To properly show detail, the growth rate scale is expanded by a factor of 2 compared to the antisymmetric case shown in Fig. 3 that follows.

But in both cases, the modes of opposite symmetry about the equator are much more unstable, so this fine structure is of limited physical significance.

Choosing a reasonable reference state density for the layer we are considering below the solar convection zone, a dimensionless toroidal magnetic field parameter $a = 1$ corresponds to peak toroidal magnetic fields of about 10^5 G. Therefore, we find instability of the system for toroidal fields as small as about 3000 G and with no apparent upper limit in a to the instability. The peak instability for the symmetric mode occurs in the neighborhood of $a = 0.15$, corresponding to a toroidal field strength of $\sim$15,000 G. The antisymmetric mode has a very broad, flat peak in growth rate for $a > 1.0$, so this occurs for toroidal fields in excess of 10^5 G.

We can see that the antisymmetric mode is considerably more unstable than the symmetric one for the same differential rotation, but this requires a considerably larger toroidal field to be realized. Thus if dynamo action is responsible for the buildup of toroidal field, then the symmetric mode of instability should be provoked first in a new magnetic cycle. It is not clear whether during such a buildup the antisymmetric mode can be realized since the reference state would already be modified during the build up phase. In the nonmagnetic case, it is the antisymmetric mode that is unstable for $s > 0.29$. Thus, weak magnetic fields excite the opposite symmetry to the nonmagnetic case.

8.2. *Phase Velocities of Unstable Disturbances*

Figures 4 and 5 show the phase velocities for the same cases as shown in Figures 2 and 3, respectively, also scaled with respect to the equatorial rotation rate. Here the $s = 0.3$ curve is the bottom one in each figure. We can see that all phase velocities fall between the minimum and maximum rotation rates for each differential rotation profile, even when the magnetic field is quite large, as anticipated in § 5 earlier. In general the higher the field strength, and the smaller the differential rotation, the closer to the equatorial rotation rate (+1.0) is the disturbance propagation speed. It is tempting to relate these rates to those observed in persistent global magnetic structures, e.g., Gaizauskas et al. (1981), and to such conventions as the "Carrington rate."

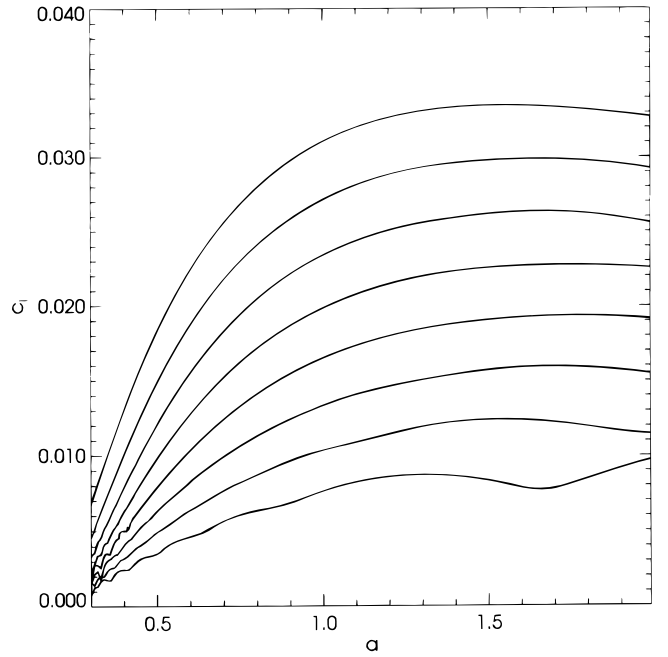

FIG. 3.—Growth rate c_i for antisymmetric modes (ψ antisymmetric, χ symmetric) as a function of toroidal field parameter a. Curves are for differential rotation parameter values $s = 0.30$–0.09 in decrements of 0.03, with $s = 0.30$ having the highest growth rate. Note that the growth rate scale is contracted by a factor of 2 compared to the symmetric case in Fig. 2.

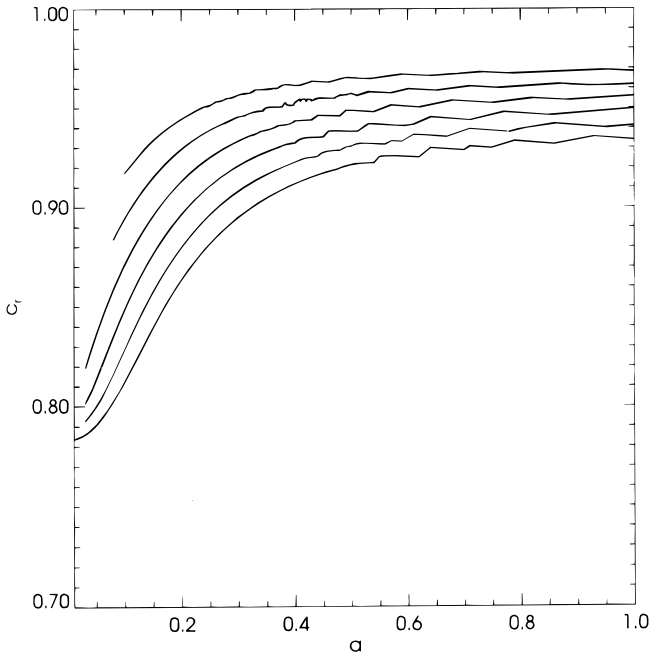

FIG. 4.—Phase velocity c_r for symmetric modes for same parameter values as in Fig. 2. For all a, $s = 0.18$ has the highest phase velocity, $s = 0.30$ the lowest.

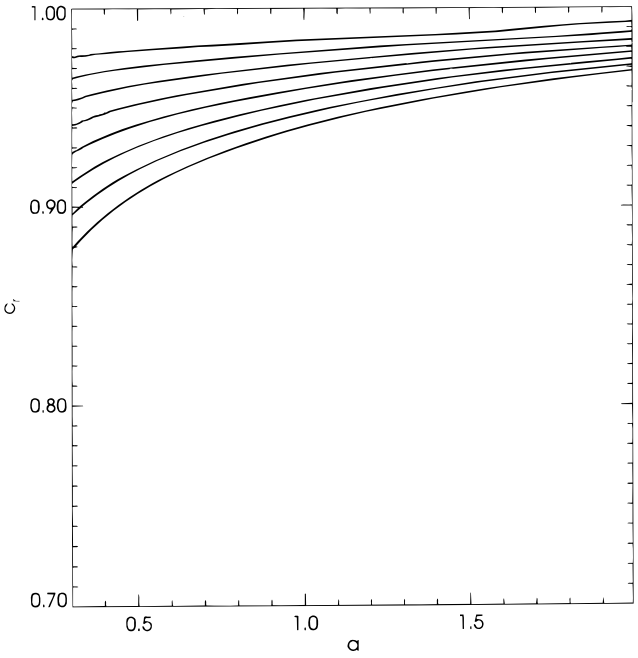

FIG. 5.—Phase velocity c_r for antisymmetric modes for the same parameter values as in Fig. 3. For all a, $s = 0.09$ has the highest phase velocity, $s = 0.30$ the lowest.

8.3. *Properties of a Typical Symmetric Case*

We illustrate in Figures 6–11 properties of an unstable solution for which ψ is symmetric and χ antisymmetric about the equator. We choose the case $s = 0.24$, $a = 0.15$, about in the middle of the growth rate ridge seen in Figure 2. Figure 6 demonstrates the degree of convergence of this solution. Plotted here are the squared amplitudes of the eigenvector coefficients of the associated Legendre polynomials, as a function of the summation index n (this particular solution was truncated at $n = 150$, a common choice). The velocity stream function amplitude is represented by the solid curve, the analogous magnetic function by the dashed curve.

Several features are immediately evident. First, the ψ amplitudes start with $n = 3$ rather than $n = 1$. This is because Ψ_1^1 is virtually zero. All symmetric solutions we have examined have this trait, indicating total suppression of stream line patterns that have no node between equator and pole. Second, the squared amplitude in the eigenvector declines by about 10 orders of magnitude by $n = 150$, representing excellent convergence. Third, above $n = 10$ or so, the two squared amplitudes are virtually the same, indicating that the finer details of the perturbations in velocity and magnetic fields are in a state of equipartition of energy. This is a common characteristic of symmetric modes, for which a is not large. Finally, there is fine structure in the curves near the truncation point, which represents a limitation of the solution method. (Taking $n = 200$ in this case moves the fine structure further to the right and decreases its amplitude further but at the expense of a considerably longer computation.) In this particular case, this high frequency "noise" has no practical effect on the solutions, even out to second order in amplitudes and derivatives.

The complete perturbation patterns for ψ_s and χ_a as functions of latitude and longitude are shown in Figure 7. The amplitude of the contour levels are the same for kinetic and magnetic perturbations. We see that the disturbances in velocity and magnetic field are truly global but with the magnetic pattern for this case largely confined poleward of 25° latitude. The velocity stream function has two nodes between equator and pole, consistent with the first eigenvector element being Ψ_3^1 rather than Ψ_1^1. One feature to note particularly in both these patterns are the "tilts" in the

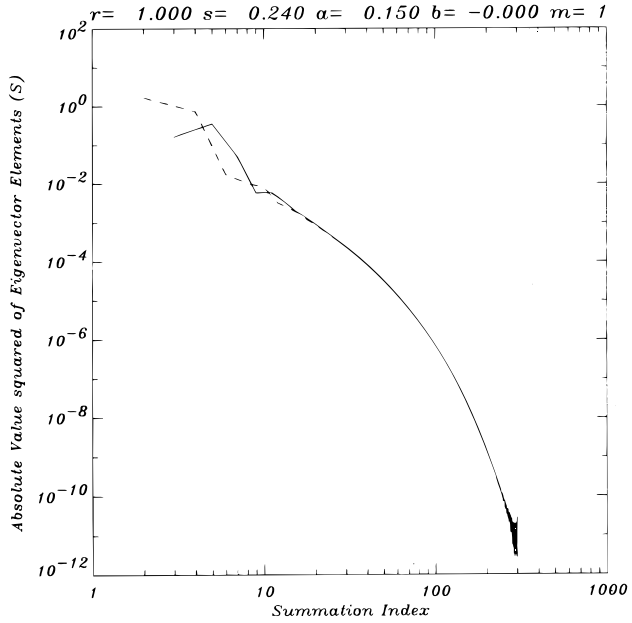

FIG. 6.—Square of eigenvector amplitude as a function of summation index, for specific symmetric mode solution with $s = 0.24$ and $a = 0.15$. Solid curve represents $|\psi|^2$ elements; dashed curve $|\chi|^2$ elements. Both are normalized to the same factor, namely, the maximum of the absolute value of the eigenfunction. For the symmetric mode, the summation index $n = 1$ amplitude in ψ is zero, to the accuracy of our calculation, or at $-\infty$ on the log scale used, and so is omitted from the plot of the solid line.

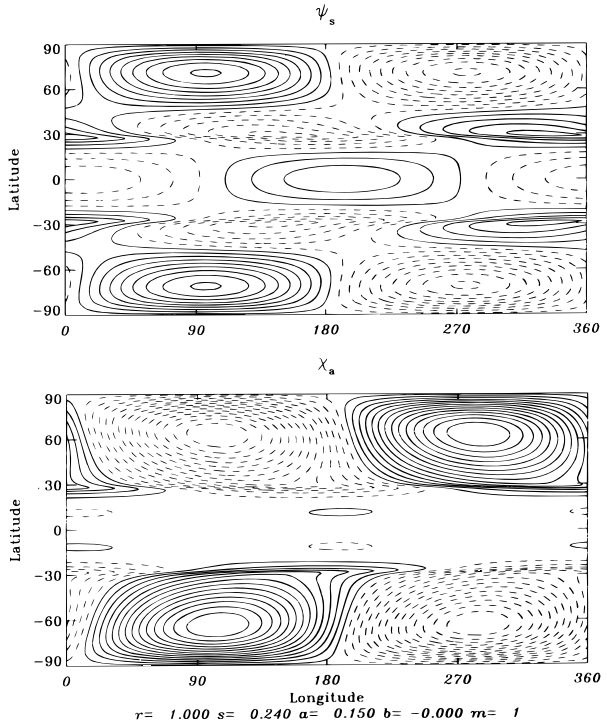

FIG. 7.—Planform of eigenfunctions ψ_s and X_a (the symmetric mode), for $s = 0.24$, $a = 0.15$: contours have same units on both plots.

contours, toward lower longitude with increasing latitude. These are particularly pronounced in both streamlines and field lines in the neighborhood of 30° latitude. These tilts imply correlation between the perturbation velocities u' and v', and between perturbation magnetic fields a' and b', so that both the Reynolds stress $\overline{u'v'}$ and the Maxwell stress $\overline{a'b'}$ are nonzero. As discussed in § 7, this is what is required (with the right sign) to extract energy from the differential rotation profile to drive the instability.

The sense of the tilt seen in Figure 7 is such that in these solutions the Reynolds stress is transporting momentum predominantly toward the equator, while the Maxwell stress is transporting it toward the poles. This is verified by Figure 8, which plots separately these two stresses against sin (latitude). The sum of these two is shown in Figure 9, which represents the total stress $\overline{u'v'} - \overline{a'b'}$. We see here that the Reynolds and Maxwell stresses counterbalance in such a way as to produce a broad smooth transport of momentum toward the poles in each hemisphere, which is exactly what is needed to extract energy from the differential rotation to drive the instability. It is clearly the Maxwell stress that dominates because the Reynolds stress by itself seen in Figure 8 would transport momentum toward the equator, tending to build up the differential rotation. Thus the Maxwell stress is key to making the differential rotation unstable whereas without a toroidal field present, it would be stable, as Watson (1981) showed.

Equation (15) indicates that the differential rotation profile will change from the unperturbed state according to the divergence or convergence in latitude of the total transport of angular momentum by the two stresses. Given the profile of this transport implied in Figure 9 we should expect particularly sharp changes in rotation at the equatorward edge of the sum of the stresses, i.e., where this sum changes rapidly. The second order solution (equations [15], [16]) for these changes is shown in Figure 10, and we see that the dominant feature is a pair of retrograde jets right at

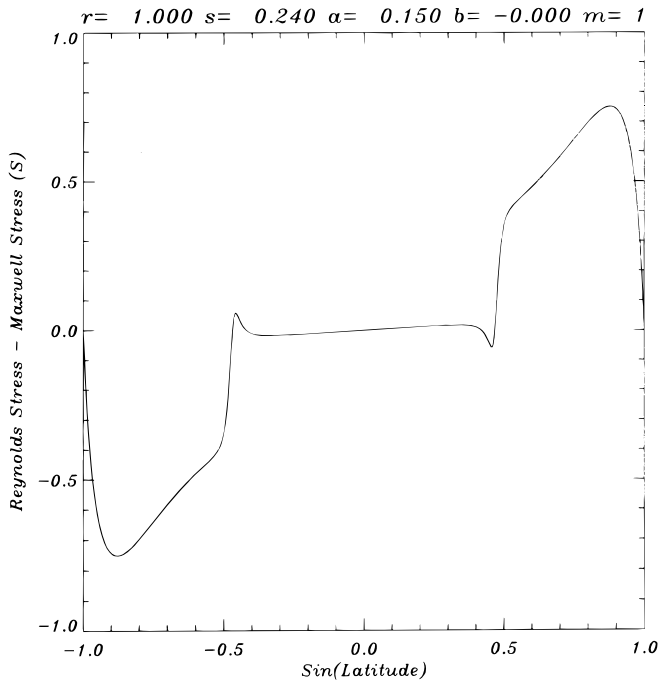

FIG. 9.—Sum of stresses shown individually in Fig. 8

this edge, with weaker prograde features both poleward and equatorward of this jet. The dominant result is that angular momentum is extracted from a narrow band of latitude near 30° latitude and deposited in latitudes above about 45°. Polar regions are seen to spin up significantly.

There is no way to predict from the second-order theory for the initial tendency how large in amplitude such jets might become, but it is tempting to speculate that they may be related to the so-called torsional oscillations on the sun, as well as to anomalous polar rotation rates, as seen for example in rotation of certain magnetic features (Snodgrass

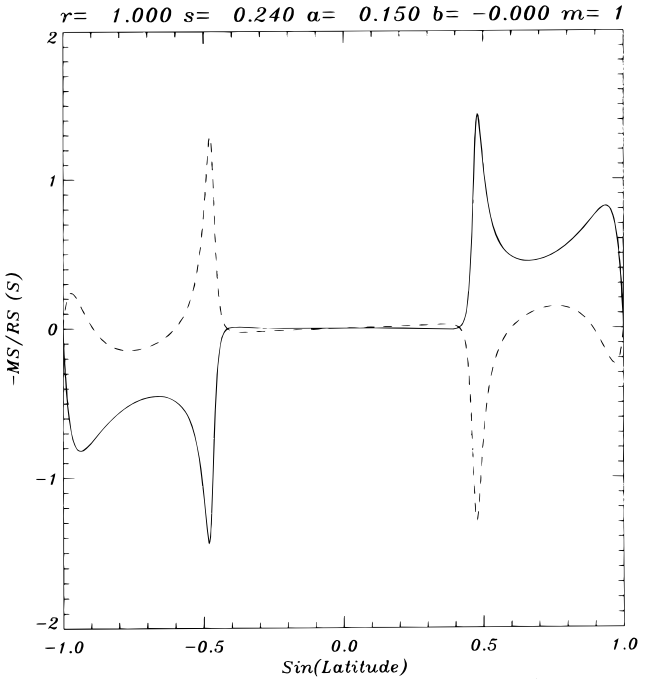

FIG. 8.—Negative of Maxwell stress (*solid curve*) and Reynolds stress (*dashed curve*) for same solution as in Fig. 7.

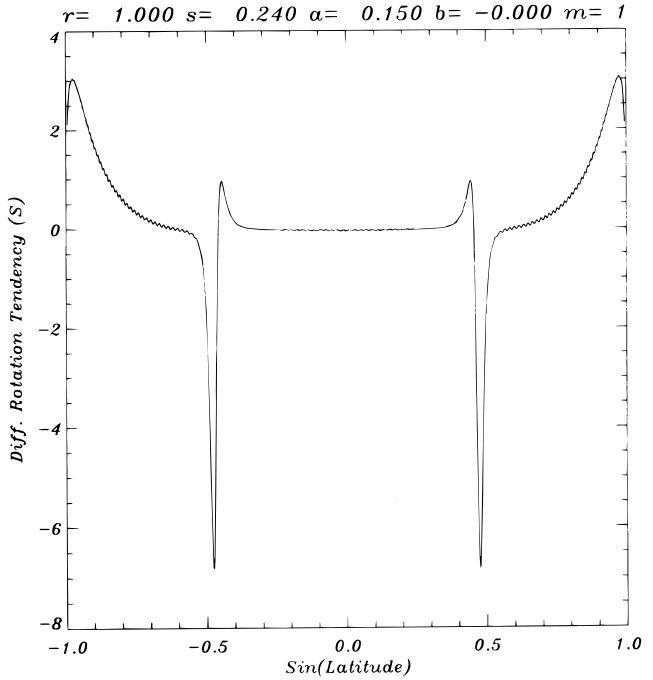

FIG. 10.—Initial change in differential rotation linear velocity due to stresses shown in Fig. 9.

1992). We will return to this point when we have illustrated further characteristics of the solutions.

A second prominent feature of the perturbation planforms seen in Figure 7 is the phase difference in longitude between the flow and field streamlines. If the two patterns coincided, with or without tilts with latitude, then the mixed stress $\overline{u'b'} - \overline{v'a'}$. needed by equation (16) to change the reference state toroidal field, would vanish, and no net transport of magnetic flux in latitude could occur, so $\bar{a}$ would not change. In fact the phase shifts are largest and changing most rapidly in the neighborhood of 30° latitude, as with the tilts. This results in an initial tendency for the toroidal field $\bar{a}$ to change according to the pattern shown in Figure 11. Given that in each hemisphere, the peak reference state toroidal field is at 45° latitude, Figure 11 implies that toroidal flux is being increased where it is lower than average and decreased where it is higher than average. This is occurring principally near 30° latitude. Therefore, energy is being extracted from the reference state toroidal field to help drive the instability, as predicted for $b = 0$ field profiles by equation (32). In addition, the polar toroidal field is being decreased from its reference state value.

As with the differential rotation changes discussed earlier, we cannot determine from these calculations the amplitude of the change in toroidal field. But as with the rotation changes, it is tempting to speculate that the sharp features of Figure 11, if they occur in the sun, provide a preferred location in an otherwise broad toroidal field for more concentrated flux to occur that might be more likely to spawn rising loops that reach the photosphere as sunspots and active regions. The polar changes may participate in the process of polar field reversal since the initial tendency in the toroidal field always opposes the reference state profile, at a latitude where it is already weak compared to midlatitudes.

Figures 10 and 11 both show very small scale structure in the profiles. These arise from the high n terms in the eigenvector, that are noisy in Figure 6, when the discritized [typically 720 points in sin (lat)]-eigenfunction is differentiated twice in latitude to compute the right-hand sides of equations (15) and (16). For $n = 150$ truncation, the amplification factor is of order 2×10^4 in amplitude since the derivative of an associated Legendre polynomial of latitude index n is of order n times the polynomial. From Figure 6, the eigenvector amplitudes near $n = 150$ are of order 10^5 smaller than for low n, so this amplification factor can produce a visible effect.

The patterns of the growing perturbations seen in Figure 7 are typical of disturbances of this symmetry for moderate toroidal field parameter a. For the same differential rotation parameter s, but a smaller than the $a = 0.15$ case shown, the patterns are similar. However, the smaller is a, the more the tilted patterns are confined to higher latitudes. For $a = 0.05$, for example, there is no significant tilt equatorward of about 50° latitude. Consequently, the second-order changes in rotation and toroidal field are found in higher and higher latitudes also. Conversely, for $a > 0.15$, the perturbation magnetic fields in particular spread toward the equator, and the stress profile seen in Figure 9 gets broader still, so the changes to the reference state toroidal field and differential rotation are found in still lower latitudes.

Disturbance planforms are less sensitive to changes in s for a given a. Patterns for $s = 0.29$ and 0.19 are fairly close to those for 0.24, with some tendency to spread toward the equator for higher s, and retreat toward the pole for lower s.

8.4. *Energetics of Symmetric Cases*

From Figures 2 and 3, symmetric modes dominate in the instability from $a \sim 0$ to 0.3 or 0.4, depending on s. This range of a implies a large change in the relative energies stored in the reference state differential rotation ($\bar{K}$) and toroidal field ($\bar{M}$). This can be seen for $s = 0.24$ in Figure 12, which depicts the fractions of the total reference state energy in each. The case $a = 0.15$ we have studied in detail

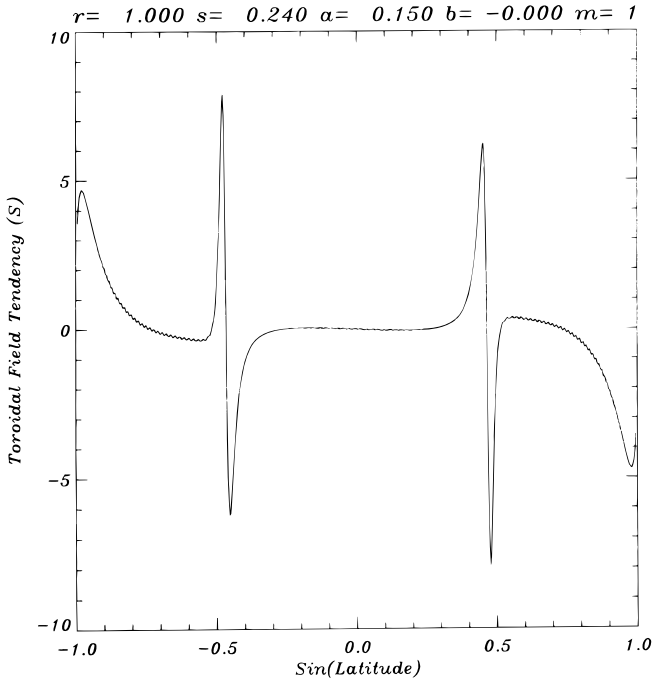

FIG. 11.—Initial change in toroidal field for same case as shown in Figs. 8–10.

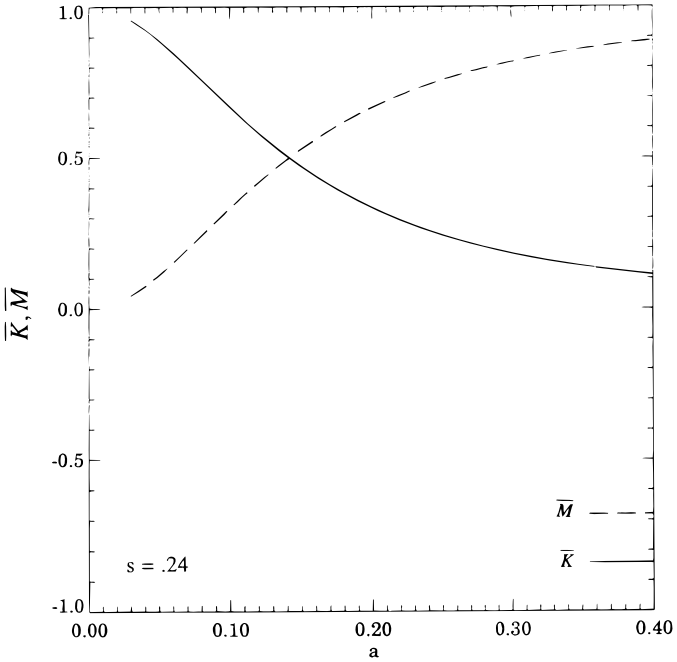

FIG. 12.—Relative energies in reference state, as a function of toroidal field parameter a, for $s = 0.24$, that are acted upon by symmetric mode perturbations.

above is near the equipartition point between kinetic and magnetic energies. By contrast, at $a = 0.05$ about 90% of the reference state energy is kinetic, and at $a = 0.4$, 90% is magnetic. From these differences we might expect that the energy conversion rates defined and discussed in § 7 will vary substantially in relative importance, as may the relative energies in the kinetic and magnetic perturbations.

Figure 13 shows the relative energies in the kinetic (K') and magnetic (M') perturbations for symmetric modes with $s = 0.24$. We see that, as we might expect, at the high a end, perturbation magnetic energy dominates over perturbation kinetic energy. There is more magnetic energy in the reference state reservoir, which is released into the perturbations. The mechanics of this are more subtle because, from Figure 1 and associated discussion, reference state magnetic energy cannot be transformed directly into perturbation magnetic energy: it must first go through a kinetic energy reservoir. Which reservoir depends on parameter values, as we shall show shortly.

For small values of a, for which the kinetic energy reservoir is much larger (Fig. 12), the behavior is different. Here, the perturbation kinetic and magnetic energies approach equipartition rather than being dominated by kinetic energy. If kinetic energy did dominate, then we would essentially be back to an instability in which magnetic fields played little role—but then Watson's results should apply, and the differential rotation, even though it is the large reservoir, would be stable. Equipartition is to be expected because as a approaches 0, the growth rate gets small since it must go to zero in the limit, given Watson's result. With equipartition, and both kinetic and magnetic disturbance planforms shrinking toward the pole, the Maxwell and Reynolds stresses cancel each other more and more closely, reducing the ability of the disturbance to extract energy from the differential rotation and grow.

The energy conversions defined in § 7 are shown in detail for the symmetric $s = 0.24$ solutions in Figure 14. Here all

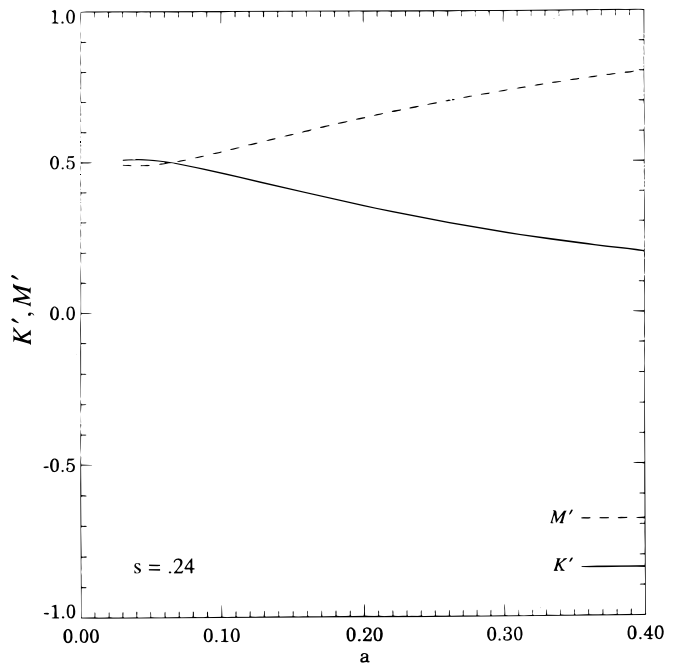

FIG. 13.—Relative energies in symmetric mode perturbations for same cases as in Fig. 12.

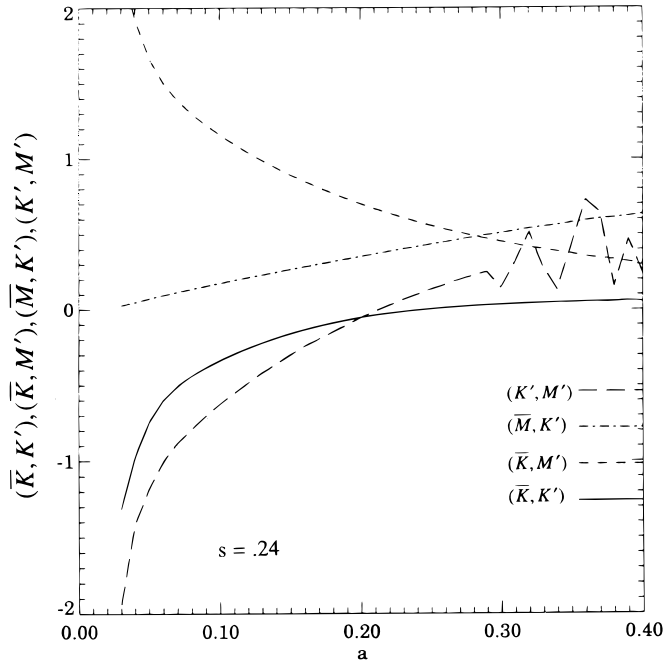

FIG. 14.—Relative energy conservation rates for symmetric modes with $s = 0.24$ as a function of toroidal field parameter a. Definitions in the text of § 4.

conversion rates have been normalized by the total rate at which energy is extracted from the reference state. Positive values then represent sources for the perturbations, negative values are sinks. With this normalization, the sum of ($\bar{K}$, K'), ($\bar{K}$, M') and ($\bar{M}$, K') curves (*solid*, *short-dashed*, and *dot-dashed* curves) should always add up to $+1$, and inspection shows that they do. Figure 14 verifies that at all $a < 0.3$ or so, work done by the Maxwell stress on the differential rotation is the primary energy source for the instability, with work done by the Reynolds stress always opposing it. (That is, the short-dashed curve is the most positive, and the solid curve is negative.) For very small a, both work terms get large in amplitude, though opposite in sign because they are normalized essentially by their sum, which is approaching zero. For increasing a, we see also that the extraction of energy from the toroidal field profile by mixed stress is increasingly important. By $a = 0.4$, almost two-thirds of the energy for perturbation growth comes from this source. Also, the Reynolds stress work term becomes slightly positive, so the Reynolds and Maxwell stresses no longer oppose each other, although both are relatively weak.

The fourth curve in Figure 14 is the energy conversion between perturbation magnetic and kinetic energies, due to the latitude component of the perturbation $\boldsymbol{j} \times \boldsymbol{B}$ force. This conversion process allows the kinetic and magnetic perturbations to grow at the same rate even when the relative amplitudes are quite different. Accordingly, at low a, perturbation magnetic energy created by the Maxwell stress is converted into perturbation kinetic energy, while for higher a, perturbation kinetic energy created by the mixed stress acting on the reference state toroidal field is converted into perturbation magnetic energy. The fluctuations in this conversion rate between $a = 0.3$ and 0.4 are another manifestation of the fine structure in the growth rates seen in Figure 2 and the high-frequency noise illustrated in Figure 6. For perturbations of this symmetry, convergence is increasingly

difficult to achieve as a is increased through this range as the growth rate gets small and fluctuates rapidly with a. The second derivatives in this particular diagnostic of the solution are the most sensitive to this problem. The eigenfunction and its first derivative are much better behaved, as illustrated by the smoothness of the other diagnostics.

8.5. *Properties of a Typical Antisymmetric Case*

As is evident from Figures 2 and 3, for $a > 0.4$ the antisymmetric mode has the larger growth rate, which becomes much larger than for any symmetric mode by $a = 0.8$. Figure 15 illustrates a typical antisymmetric case, again for $s = 0.24$, with $a = 0.8$. The important features are the dominance of the magnetic perturbations, the completely global extent of both kinetic and magnetic features, and the substantial phase differences in longitude between the flow and field streamlines. Even though the velocities are relatively weak, they are essential for extracting energy from the toroidal field through the mixed stress. The Reynolds and Maxwell stress profiles, seen in Figure 16, are qualitatively similar to the symmetric case for lower a but with the peaks in both moved to quite low latitudes. The net stress profile, shown in Figure 17, shows a very broad pattern of momentum transport toward the poles, with a small reversal very near the equator. This feature disappears for still higher a. The second order changes in differential rotation that result from this stress profile are seen in Figure 18, showing a jet structure within a few degrees on both sides of the equator. (Changes in differential rotation are symmetric about the equator for both symmetry pairs of ψ and χ.) The corresponding toroidal field change is seen in Figure 19. (Changes in toroidal field are antisymmetric about the equator for both symmetry pairs of perturbations.)

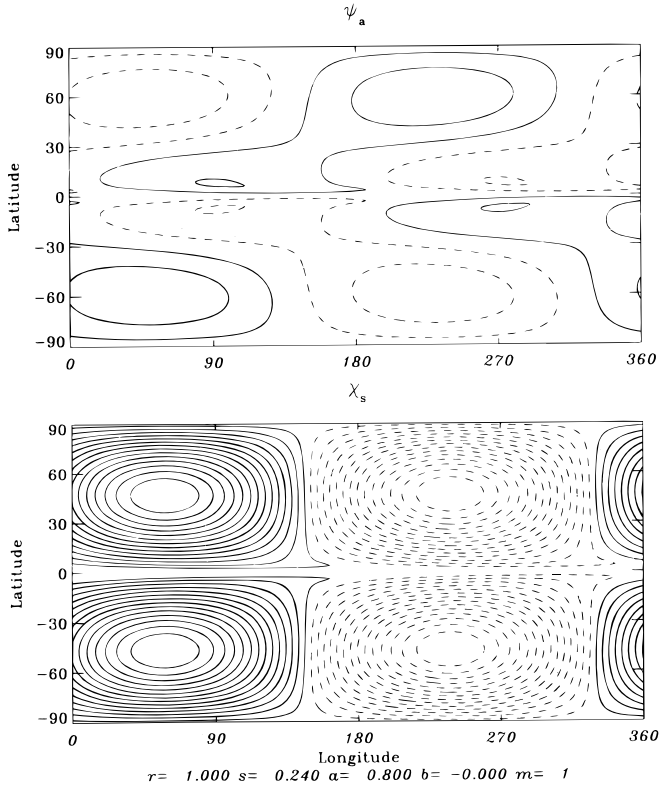

FIG. 15.—Planform of eigenfunctions ψ_a, χ_s (the antisymmetric mode), for $s = 0.24$ and $a = 0.80$. Contours have the same units on both plots.

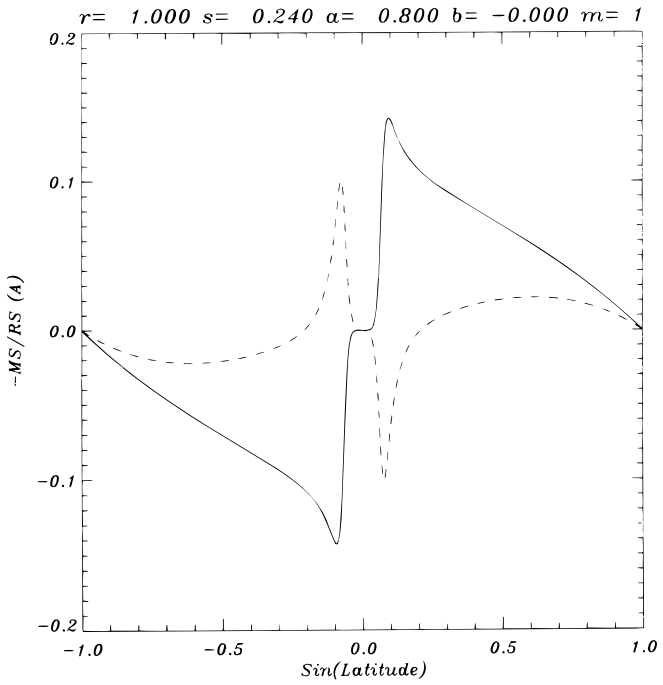

FIG. 16.—Negative of Maxwell stress (*solid curve*) and Reynolds stress (*dashed curve*) for same solution as in Fig. 15.

Since χ is symmetric about the equator the planform for the magnetic perturbations seen in Figure 15 imply that perturbation east-west field of opposite signs are being brought together at the equator since $a' \sim \partial\chi/\partial\mu$. With the addition of even a small amount of ohmic diffusion, this pattern could be a site of magnetic reconnection that could help destroy flux near the end of a magnetic cycle on the sun.

8.6. *Energetics of Antisymmetric Cases*

The energetics for these unstable modes are considerably simpler than for the symmetric modes with small a. Figure

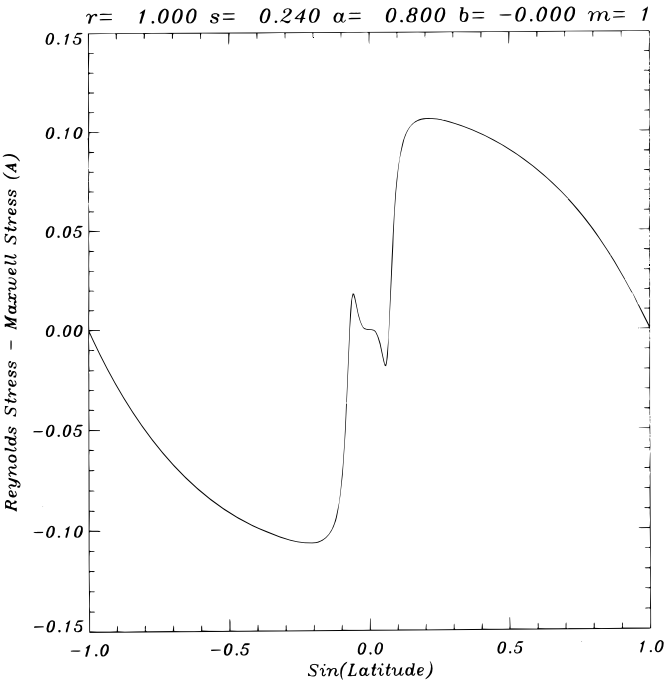

FIG. 17.—Sum of stresses shown in Fig. 16

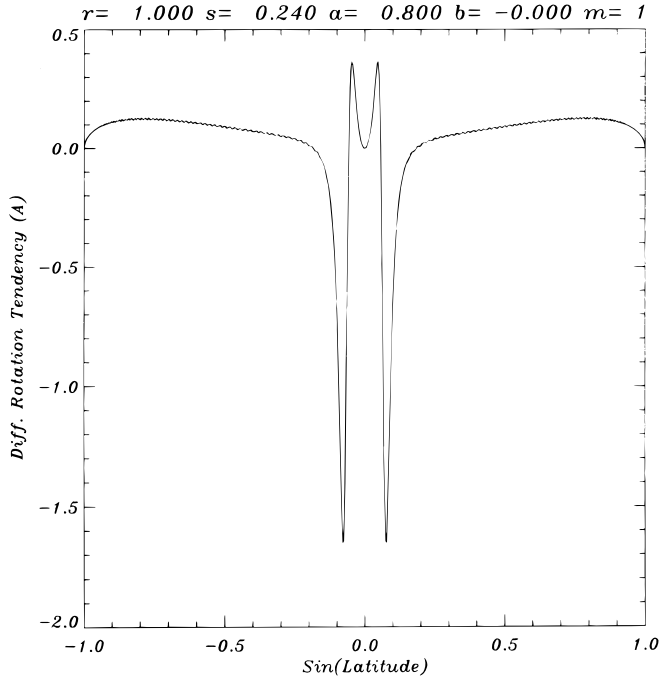

FIG. 18.—Initial change in differential rotation linear velocity due to stresses shown in Fig. 17.

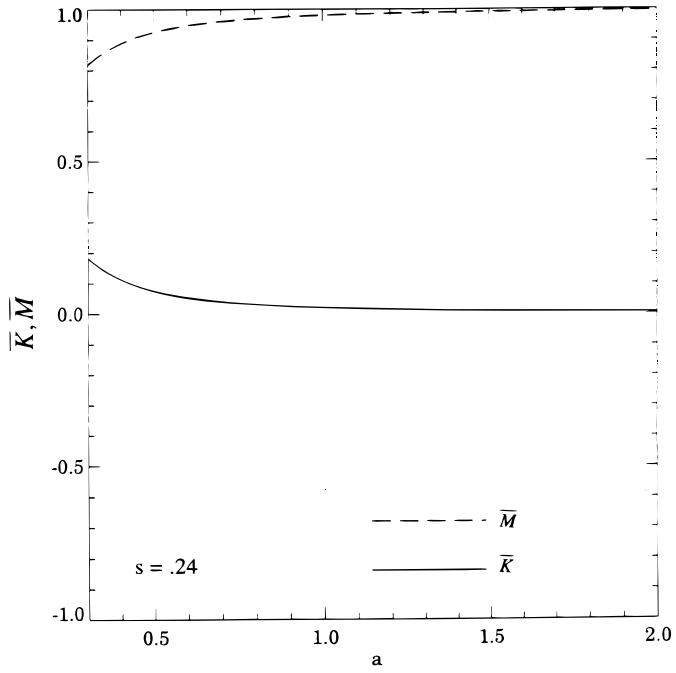

FIG. 20.—Relative energies in reference state, as a function of toroidal field parameter a, for $s = 0.24$, that are acted upon by antisymmetric mode perturbations.

20 shows the relative kinetic and magnetic energies in the reference state for a values large enough for the antisymmetric mode to be the fastest growing. By $a = 0.8$, 98% or so of the energy is in magnetic form. A plot of relative perturbation energies (not shown) for this a range looks essentially the same. The relative energy conversion rates among the various reservoirs, analogous to Figure 14 for symmetric modes, is shown in Figure 21. This shows the growing dominance of energy extracted from the toroidal field by the mixed stress as a increases, and the waning of both Reynolds and Maxwell stresses acting on the differential rotation. The near coincidence of $(\bar{M}, K')$ and (K', M') approaching $+1$ shows that virtually none of the energy extracted from the toroidal field remains as perturbation kinetic energy but is immediately converted to perturbation magnetic energy by the perturbation $\boldsymbol{j} \times \boldsymbol{B}$ force. Hence the dominance of magnetic over velocity contours in Figure 15, which is even more extreme for $a > 0.8$, the case shown. The plot for (K', M') is much smoother than in the symmetric

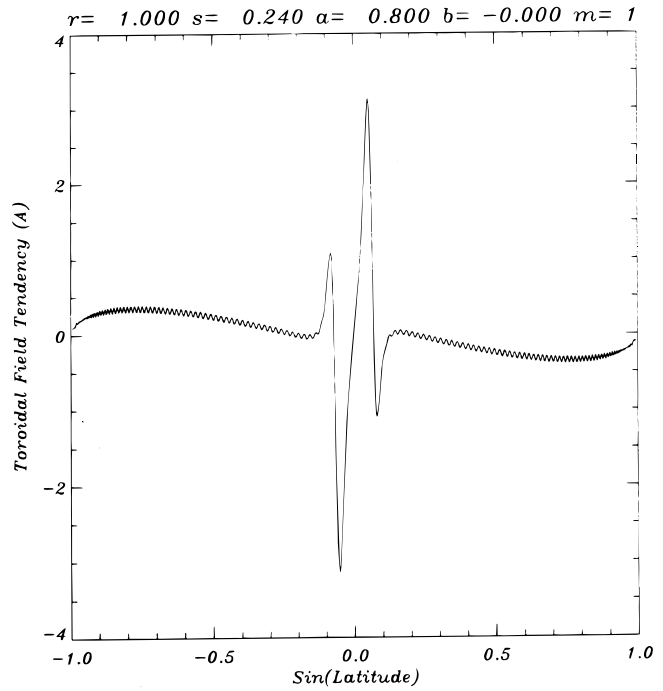

FIG. 19.—Initial change in toroidal field for same case as shown in Figs. 15–17.

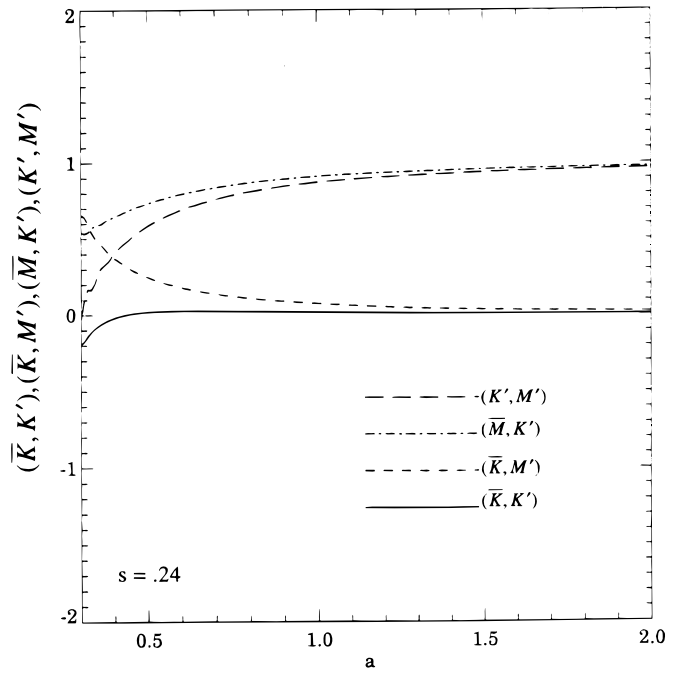

FIG. 21.—Relative energy conversion rates for antisymmetric modes with $s = 0.24$ as a function of toroidal field parameter a. See definitions in the text of § 7.

case shown in Figure 14 because the antisymmetric case is very well converged even at high values of a.

8.7. *Latitudes of Initial Changes in Differential Rotation and Toroidal Field*

We have shown two detailed examples of the second-order initial changes in differential rotation and toroidal field that the stresses associated with growing modes would induce. In Figure 22 we plot the latitude positions for the peaks in these changes for modes of both symmetries, for a large number of cases computed for $s = 0.21$ and 0.27, bracketing the detailed examples we gave earlier in Figures 10, 11, 18, and 19. We see that these latitudes span the full range of sunspot latitudes, and beyond. The important feature is that as the magnetic field parameter increases, the latitude decreases, so we can imagine that if the instability we have demonstrated occurs in the sun, as the toroidal field of a new cycle builds up, these disturbances appear and migrate toward the equator, reminiscent of both the torsional oscillations and the butterfly diagram. Whether these solution characteristics are really related to these solar phenomena can only be determined by nonlinear dynamo-type modeling that allows the instability to occur, coupled with more sensitive inferences from helioseismology of the dynamics and magnetic structure of the shear layer at the base of the convection zone.

We also point out that the symmetries of the induced changes in differential rotation and toroidal field about the equator are the same—differential rotation symmetric, toroidal field antisymmetric—for both the symmetric case ψ_s, χ_a and the antisymmetric case ψ_a, χ_s. To produce a departure from this symmetry pattern requires perturbations of both symmetry pairs to be present, something that can be produced only in a nonlinear model.

8.8. *Dominant Energy Flows in Unstable Modes*

We can summarize the energetics of unstable modes rather simply, capturing the basic characteristics of many solutions not shown in detail. In particular, for low a for which symmetric modes grow fastest, the dominant energy flow is

$$\bar{K} \rightarrow M' \rightarrow K' \rightarrow \bar{K} \ .$$

In words, the Maxwell stress converts differential rotation energy into perturbation magnetic energy, some of which the perturbation latitudinal $\boldsymbol{j} \times \boldsymbol{B}$ force transforms into perturbation kinetic energy. Some of that finally is put back into the differential rotation by the Reynolds stress. The last step is weakly reversed for a close to the upper limit for symmetric growing modes that amplify faster than antisymmetric modes for the same parameter values.

For larger a, for which antisymmetric modes grow fastest, the dominant energy path is

$$\bar{M} \rightarrow K' \rightarrow M' \ .$$

In words, here the mixed stress converts toroidal field energy into perturbation kinetic energy, almost all of which is further converted by the latitudinal $\boldsymbol{j} \times \boldsymbol{B}$ force into perturbation magnetic energy. The net result is a magnetically dominated instability, from the original reservoir to the growing perturbations.

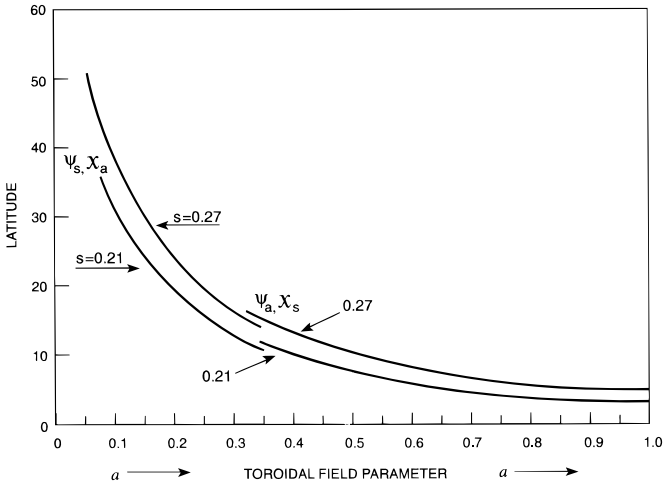

FIG. 22.—Summary plot of latitudes at which peaks in changes in reference state differential rotation and toroidal field occur, for both symmetric (ψ_s, χ_a) and antisymmetric (ψ_a, χ_s) modes, for differential rotation parameters $s = 0.27$ and 0.21. Consistent with the growth rates shown in Figs. 2 and 3, the symmetric mode leads to the pair of curves in the range $0 < a \lesssim 0.35$; the antisymmetric mode to curves for $a > 0.35$. Peaks in induced differential rotation and toroidal field shown in Figs. 10, 11, 18, and 19 for $a = 0.15$ and 0.8 with $s = 0.24$ would fall neatly inbetween the pairs of continuous curves shown.

9. COMMENTS AND CONCLUSIONS

The principal conclusion we draw from these calculations is that solar-type differential rotation profiles of virtually any magnitude are unstable to two-dimensional perturbations when a broad toroidal field is present. Instability occurs for almost any magnitude of toroidal field, with the field supplying the energy when it is large, and the differential rotation supplying the energy when the field is small. What varies with different strength differential rotation and toroidal fields is the disturbance growth rate and the dominant symmetry about the equator. When differential rotation is absent completely, there is no instability to two-dimensional disturbances, regardless of the field strength. Clearly at least a weak differential rotation is needed to produce the tilts with latitude and the phase shifts in longitude necessary for the creation of Reynolds, Maxwell, and mixed stresses that extract energy from the differential rotation and toroidal magnetic field.

The generality of this conclusion should be tested with stability calculations for other toroidal field profiles. We will report in a later paper on calculations with the parameter b not equal to zero (for which we have also found instability for virtually all b values studied), but it would also be instructive to look for instability for much more concentrated toroidal field profiles. Nevertheless, we feel the broad profiles we have studied could plausibly be produced by the differential rotation acting on a broad poloidal field as part of the solar dynamo.

Since the unstable disturbances are strictly two-dimensional, they cannot produce a dynamo, even in concert with the differential rotation. They could contribute significantly to a dynamo that has additional processes at work, particularly those that produce radial magnetic flux. While the fully three-dimensional problem is much more difficult, there is an intermediate step that allows introduction of enough three-dimensional features to, in principle, sustain a dynamo, while still solving only two-dimensional equations. This intermediate step involves the hydromagnetic generalization of the so-called "shallow-

water" equations that have been used extensively for the global fluid dynamics of the atmosphere and oceans. This system will be developed in a later paper. Such a system would allow for generation of a longitude-independent poloidal field which could be sheared by the differential rotation to change the toroidal field.

Even without the third dimension, it is of interest to calculate how large the unstable disturbances become and how much they modify the reference state. Without doing detailed calculations, we estimate by analogy with other nonlinear fluid systems that the nonlinearities could modify the differential rotation by a few tens of percent, on timescales of months to years. If so, then helioseismology may be able to detect the presence of this instability at the base of the solar convection zone. We have found instability only for longitudinal wavenumber 1, but in the nonlinear case we should expect higher longitudinal wavenumbers to be excited, through wave interactions.

The thickness of the layer at the convection zone base that contains the toroidal field is not known from observations, but there are reasons to believe that it contains fields of strength perhaps 5×10^4 G, with a thickness no greater than several thousand kilometers. The high field strength is needed to get the flux loops to overcome the effect of coriolis forces and emerge at low latitudes where the butterfly diagram is formed (Choudhuri & Gilman 1987; Fisher et al. 1994, and references therein). For field strengths this high, if the layer of high fields is as much as a few tens of thousands of kilometers thick, then there would be too much flux rising to the surface in a sunspot cycle since there is no obvious mechanism for preventing it from rising. This consideration leads to the presumption that not that much is there (Galloway & Weiss 1981).

It is sometimes argued that dynamo action should be suppressed when the induced fields approach or exceed equipartion of energy with the inducing motions. But it is known that the so-called interface dynamos (Parker 1993; Charbonneau & MacGregor 1996) can sustain toroidal fields that exceed equipartition in the low ohmic diffusion part of the domain. Also, the instability we have demonstrated is actually enhanced, not suppressed, by strong toroidal fields. In fact, the instability itself may disrupt the build-up of toroidal fields beyond some point that can only be determined by nonlinear calculations.

The authors wish to thank Boon Chye Low for reviewing the entire manuscript, and also Mausumi Dikpati and Paul Charbonneau for their comments. Thanks also to Louise Beierle for preparing the manuscript.

APPENDIX A

A.1. NECESSARY CONDITION FOR INSTABILITY

This condition was derived from equation (17) by multiplying by ψ^*, integrating from pole to pole, integrating by parts, and separating out the imaginary part of the result:

$$c_i \int_{-1}^{1} \left(\left\{ -\frac{[\omega_0(1-\mu^2)]''}{|\omega_0 - c|^2} + \frac{2(\omega_0 - c_r)}{|\omega_0 - c|^4}\left[\frac{m^2\alpha_0^2}{(1-\mu^2)} - \frac{1}{\mu}(\mu^2\alpha_0^2)'\right] + \frac{[3(\omega_0 - c_r)^2 - c_i^2][(1-\mu^2)\alpha_0^2\,\omega_0']'}{|\omega_0 - c|^6} - \frac{8(\omega_0 - c_r)[(\omega_0 - c_r)^2 - c_i^2]\alpha_0^2(\omega_0')^2}{|\omega_0 - c|^8} \right\} |\psi|^2 + \frac{2(\omega_0 - c_r)(1-\mu^2)\alpha_0^2}{|\omega_0 - c|^4}|\psi'|^2 \right) d\mu = 0 ,$$

where the primes denote differentiation with respect to μ. This implies that for $c_i \neq 0$, integral must vanish over the domain.

A.2. RECURSION RELATIONS FOR COEFFICIENTS IN LEGENDRE POLYNOMIAL EXPANSION AND THEIR ASSOCIATED MATRICES

Assuming $\omega_0 = r - s\mu^2$, $\alpha_0 = a\mu + b\mu^3$, substitution into equation (23) and requiring the coefficients of like Legendre polynomials to vanish yields the recursion relation

$$R_n \Psi_{n-2} + S_n \Psi_n + T_n \Psi_{n+2} + K_n X_{n-3} + L_n X_{n-1} + M_n X_{n+1} + N_n X_{n+3} = -c\Psi_n . \tag{A1}$$

Doing the same with equation (24) yields

$$E_n \Psi_{n-3} + F_n \Psi_{n-1} + G_n \Psi_{n+1} + H_n \Psi_{n+3} + A_n X_{n-2} + B_n X_n + C_n X_{n+2} = -cX_n . \tag{A2}$$

In the above, the coefficients of the Ψ's are

$$E_n = b\frac{(n-m-2)(n-m-1)(n-m)}{(2n-5)(2n-3)(2n-1)}, \qquad R_n = \frac{s[(n-2)(n-1)-12](n-m-1)(n-m)}{n(n+1)(2n-3)(2n-1)},$$

$$F_n = \frac{a(n-m)}{(2n-1)} + \frac{3b(n-m)[(n-1)(n+1)-(m^2+1)]}{(2n-3)(2n-1)(2n+3)}, \qquad S_n = -r + \frac{2(r+s)}{n(n+1)} + s\frac{[2n(n+1)-1-2m^2]}{(2n-1)(2n+3)n(n+1)},$$

$$G_n = \frac{a(n+m+1)}{2n+3} + \frac{3b(n+m+1)[(n+1)^2-2-m^2]}{(2n-1)(2n+3)(2n+5)}, \qquad T_n = \frac{s[(n+2)(n+3)-12](n+m+2)(n+m+1)}{n(n+1)(2n+3)(2n+5)},$$

$$H_n = b\frac{(n+m+3)(n+m+2)(n+m+1)}{(2n+3)(2n+5)(2n+7)},$$

and the coefficients of the X's are

$$K_n = \frac{b[(n-3)(n-2)-20](n-m-2)(n-m-1)(n-m)}{n(n+1)(2n-5)(2n-3)(2n-1)}, \qquad A_n = s\,\frac{(n-m-1)(n-m)}{(2n-3)(2n-1)},$$

$$L_n = \frac{[(n-1)na + 6(b-a)](n-m)}{n(n+1)(2n-1)} + 3b\,\frac{[(n-1)n-20](n-m)[(n-1)(n-1)-(m^2+1)]}{(2n-3)(2n-1)(2n+3)n(n+1)},$$

$$B_n = -r + s\,\frac{[2n(n+1)-1-2m^2]}{(2n-1)(2n+3)},$$

$$M_n = \frac{[(n+1)(n+2)a + 6(b-a)](n+m+1)}{n(n+1)(2n+3)} + 3b\,\frac{[(n+1)(n+2)-20](n+m+1)[(n+1)^2-2-m^2]}{n(n+1)(2n-1)(2n+3)(2n+5)},$$

$$C_n = s\,\frac{(n+m+2)(n+m+1)}{(2n+3)(2n+5)},$$

$$N_n = \frac{b[(n+3)(n+4)-20](n+m+3)(n+m+2)(n+m+1)}{n(n+1)(2n+3)(2n+5)(2n+7)}.$$

Two separate matrices are formed from equations (A1) and (A2), for the two opposite symmetry pairs defined in § 6. In each case, the matrix form yields an eigenvalue equation:

$$[Q][PC] = C[PC],$$

in which [PC] represents the eigenvector, the first half of the elements of which are the Ψ's, and the second half the X's, with the series truncated at a number $n = KT$. For ψ symmetric, and χ antisymmetric, the matrix of [Q] is formed from (A1) as is, and from (A2) with the index n increased by 1. For ψ antisymmetric, χ symmetric, this matrix is formed from equation (A1) with n increased by 1, and equation (A2) as is. Then both matrix equations are solved using a standard *qr* algorithm and eigenvector routine in IDL. The elements of [Q] are real, but of course the eigenvalues and eigenvectors may be real, corresponding to neutral oscillations that generally propagate in longitude, or complex, corresponding to complex conjugate pairs of one growing and one decaying mode, that also propagate, but with phase velocities bounded according to the formulas in § 5.

In both matrices, the negatives of coefficients S and B comprise the major diagonals, with the other adjacent diagonals occupied by the negatives of the other coefficients in equations (A1) and (A2). For polynomial series truncation at $n = KT$, each matrix has dimensions $2KT \times 2KT$, and the eigenvector is of length $2KT$.

REFERENCES

Balbus, S. A., & Hawley, J. F. 1994, MNRAS, 266, 769
Brown, T. M., Christensen-Dalsgaard, J., Dziembowski, W. A., Goode, P. R., Gough, D. O., & Morrow, C. A. 1989, ApJ, 343, 526
Charbonneau, P., & MacGregor, K. B. 1996, ApJ, 473, L59
Choudhuri, A. R., & Gilman, P. A. 1987, ApJ, 316, 788
Drazin, P. G., & Howard, L. N. 1966, Adv. Appl. Mech., 9, 1
Fisher, G. H., Fan, Y., DeLuca, E. E., & McClymont, A. N. 1994, in Proc. ASP Conf. Ser. 68, Solar Active Region Evolution: Comparing Models with Observations, ed. K. S. Balasubramaniam & G. W. Simon (Utah: BookCrafters, Inc.), 109
Fjørtoft, R. 1950, Geofys. Publ. 17(6), 1
Gaizauskas, V., Harvey, K. L., Harvey, J. W., & Zwaan, C. 1983, ApJ, 265, 1056
Galloway, D. J., & Weiss, N. O. 1981, ApJ, 243, 945
Goode, P. R., Dziembowski, W. A., Korzennik, S. G., & Rhodes, E. J. 1991, ApJ, 367, 649
Kent, A. 1968, J. Plasma Phys., 2, 543
Kosovichev, A. G. 1996, ApJ, 469, L61
Kuo, H. L. 1949, J. Meteor., 6, 105
Parker, E. N. 1993, ApJ, 408, 707
Rayleigh, Lord 1880, Proc. Lond. Math. Soc., 11, 57
Snodgrass, H. B. 1992, in Proc. ASP Conf. Ser. 27, ed K. L. Harvey (Utah: BookCrafters, Inc.), 205
Speigel, E. A., & Zahn, J.-P. 1992, A&A, 265, 106
Stern, M. E. 1962, Phys. Fluids, 6, 636
Tomczyk, S., Schou, J., & Thompson, M. J. 1995, ApJ, 448, L57
Watson, M. 1981, Geophys. Astrophys. Fluid Dyn., 16, 285